

SIR-C Multifrequency Radar Backscatter Database for Terrain



Leland Pierce, M. Craig Dobson, Fawwaz Ulaby
University of Michigan

August, 2019

SIR-C Multifrequency Radar Backscatter Database for Terrain

Foreword

On two missions, in the spring and fall of 1994, the Space Shuttle carried a multi-frequency *synthetic-aperture radar* (SAR) to image large segments of planet Earth. The SAR instrument package is known as the *Shuttle Imaging Radar-C*, or **SIR-C** for short. The letter “C” refers to the fact that this particular instrument configuration was the third SAR to fly on the Space Shuttle; SIR-A was flown in 1981 and SIR-B in 1984. To date, SIR-C remains the most advanced imaging radar to fly in space. Unlike earlier missions—as well as missions flown since 1994—all of which carried single-frequency SARs, the SIR-C instrument is the only SAR to acquire backscatter data at three different frequencies, and to do so simultaneously. The SIR-C instrument included fully polarimetric SARs that operated at 1.25 GHz (L-band) and 5.3 GHz (C-band) and a non-polarimetric SAR with VV polarization at 9.6 GHz (X-band).

In support of the SIR-C mission, a team of research investigators at the University of Michigan carried out an extensive “ground-truth” survey to characterize the terrain across long swaths of the scenes imaged by the SIR-C radars. The ground-truth surveys included terrain type and associated ancillary data. This document is made available to SAR users and designers interested in quantitative information about the statistical distribution of the radar backscattering coefficient σ^0 (dB) for various types of terrain, at any of the three frequency bands operated by SIR-C. The extraction of data from the voluminous database is facilitated by the Graphical User Interface (GUI) described in detail in the sections that follow.

To commemorate the 25-year anniversary of the SIR-C mission, a team of SIR-C scientists led by Freeman [1] recently published an overview article highlighting some of the many scientific observations deduced from the SIR-C data.

List of Important Symbols

hh horizontal receive/horizontal transmit polarizations
 hv horizontal receive/vertical transmit polarizations
 vv vertical receive/vertical transmit polarizations

N = number of single-look pixels

$\sigma^{(1)}[i]$ = single-look backscattering cross-section per unit area of pixel i

$$\begin{aligned} \sigma^0 &= \langle \sigma^{(1)} \rangle \\ &\approx \frac{1}{N} \sum_{i=1}^N \sigma^{(1)}[i] = \text{backscattering coefficient, obtained by averaging over} \\ &\quad \text{a large number of pixels } N, \text{ with } i = 1 \text{ to } N. \end{aligned}$$

$$\begin{aligned} s^{(1)} &= [\langle (\sigma^{(1)} - \sigma^0)^2 \rangle]^{1/2} \\ &\approx \left[\frac{1}{N} \sum_{i=1}^N (\sigma^{(1)} - \sigma^0)^2 \right]^{1/2} = \text{single-look standard deviation} \end{aligned}$$

$$\frac{s^{(1)}}{\mu} = \frac{s^{(1)}}{\sigma^0} = \text{single-look standard deviation-to-mean ratio}$$

$$F[i] = \frac{\sigma^{(1)}[i]}{\sigma^0} = \text{single-look normalized backscattering cross-section per unit area for pixel } i$$

$T = (L1, L2, L3, L4, L5, L6)$ = terrain classification identifier

$$\sigma^0[\text{dB}] = 10 \log \sigma^0$$

$s_r^{(1)}$ = single-look radar image speckle standard deviation

$s_t^{(1)}$ = single-look terrain texture standard deviation

$R = (A1, A2, A3, N)$ = radar configuration

$$A1 = \begin{cases} 1 & \text{for L-band,} \\ 2 & \text{for C-band,} \\ 3 & \text{for X-band,} \end{cases}$$

$$A2 = \begin{cases} 1 & \text{for HH Polarization } \sigma^0 \text{ (dB) (for L- and C-bands only),} \\ 2 & \text{for VV Polarization } \sigma^0 \text{ (dB),} \\ 3 & \text{for HV Polarization } \sigma^0 \text{ (dB) (for L- and C-bands only),} \\ 4 & \text{for HH-VV Phase } \phi_{\text{hh-vv}} \text{ (for L- and C-bands only),} \end{cases}$$

$A3$ = incidence angle θ in degrees, relative to normal incidence,

N = number of looks.

Table 1: Terrain classification system.

L1 General Terrain Type	L2 Specific Terrain Class	L3 First Attribute	L4 Second Attribute	L5 Ground Condition	L6 Date	
1. Non-Vegetated	1. Urban	1. Small Town	0	0	Both Dates	
		2. Large City				
	2. Water Surface	1. Liquid	1. Calm 2. Med-Waves 3. High-Waves	0	0	Both Dates
		2. Frozen	1. Smooth 2. Rough	0	0	1. April Both Dates
	3. Paved Road		0	0	0	Both Dates
	4. Bare Soil	0	0	0	1. Wet	1. April
					2. Dry	2. October 1. April 2. October
1. Sparse Vegetation	1. Desert	1. Grasses	1	2. Dry	Both Dates	
		2. Shrubs	1	2. Dry	Both Dates	
3. Dense Vegetation	1. Wetlands	1. Grasses (flooded)	1. (Arbitrary)	1. Wet	Both Dates	
		2. Trees (flooded)	2. (Arbitrary)	1. Wet	Both Dates	
	2. Grasses/Sedges	0	1. Short ($h < 25$ cm)	1. Wet 2. Dry	1. April Both Dates	
		0	1. Tall ($h > 25$ cm)	1. Wet 2. Dry	1. April Both Dates	
	3. Shrubs	0	1. Short ($h < 1$ m)	1. Wet 2. Dry	1. April Both Dates	
		0	1. Tall ($h > 1$ m)	1. Wet 2. Dry	Both Dates Both Dates	
	4. Trees	1. Needle-Leaf	1. Short ($h < 5$ m)	1. Wet Soil	1. April	
				2. Dry Soil	2. October	
				3. Snow-Covered Soil	1. April	
			2. Tall ($h > 5$ m)	1. Wet Soil	1. April	
				2. Dry Soil	2. October	
				3. Snow-Covered Soil	1. April	
		2. Broad-Leaf	1. Short ($h < 5$ m)	1. Wet Soil	1. April	
				2. Dry Soil	2. October	
				3. Snow-Covered Soil	1. April	
			2. Tall ($h > 5$ m)	1. Wet Soil	1. April	
				2. Dry Soil	2. October	
				3. Snow-Covered Soil	1. April	
	3. Mixed	1. Short ($h < 5$ m)	1. Wet Soil	1. April		
			2. Dry Soil	2. October		
3. Snow-Covered Soil			1. April			
2. Tall ($h > 5$ m)		1. Wet Soil	1. April			
		2. Dry Soil	2. October			
		3. Snow-Covered Soil	1. April			
4. Tropical Jungle*	0	0	1. Lowland (wet soil)	Both Dates		
			2. Upland (dry soil)	Both Dates		

* Very few entries

1 Terrain Classes

The terrain classification system used in conjunction with the radar backscatter database and outlined in Table 1 consists of six levels.

Level 1 (L1): General Terrain Types, consists of three classes based on vegetation cover:

- 1 = Non-Vegetated,**
- 2 = Sparse Vegetation,** and
- 3 = Dense Vegetation.**

The non-vegetated class is subdivided into:

Level 2 (L2): Specific Terrain Classes:

- 1 = Urban,**
- 2 = Water Bodies,**
- 3 = Road Surfaces,** and
- 4 = Bare Soil.**

Further classification is provided by three levels of attributes. Sparse vegetation refers to desert terrain, which is classified at Level 3 as either **Shrubs** or **Grasses**. Dense vegetation is subdivided into four categories: **Wetlands, Grasses and Sedges, Shrubs,** and **Trees**.

The five-level terrain classification system identifies a terrain class by the sequence

$$T = (L1, L2, L3, L4, L5). \quad (1)$$

For example, the class Tall Broad-Leaf Trees with Snow-Covered Soil (observed in April 1994) is identified as $T = (3, 4, 2, 2, 3, 1)$.

2 Data Acquisition

As noted earlier, the SIR-C/X-SAR instrument was flown aboard the space shuttle twice during 1994, and in each mission it acquired polarimetric data at L- and C-bands and VV-polarized data at X-band. A large number of test sites were imaged repeatedly during a given shuttle flight and the pass-to-pass drift of the shuttle orbit provided opportunities to image a test site at a variety of angles of incidence. Many of these sites were revisited during both shuttle missions. Thus, the objectives of this study with respect to terrain classes was achieved by subsampling the data acquired by SIR-C/X-SAR during the two missions to select test sites with appropriate terrain conditions. Frequently imaged test sites in the Americas were selected to represent a range of environmental conditions ranging from wet tropical forest to temperate desert, as shown in Figure 1. Urban areas included Oklahoma City, New York and Philadelphia. For each selected test site, the available SIR-C/X-SAR data were inventoried as a function of season, date of acquisition, viewing geometry, and the sensor configuration (frequency and polarization). Examples of this inventory are given in Table 2 for several of the test sites. All SIR-C/X-SAR scenes acquired in polarimetric mode at both L- and C-bands were ordered and processed to single-look by the EROS Data Centre in Sioux Falls, South Dakota. This amounted to 152 scenes at each frequency. These data were received, displayed and checked for image quality.

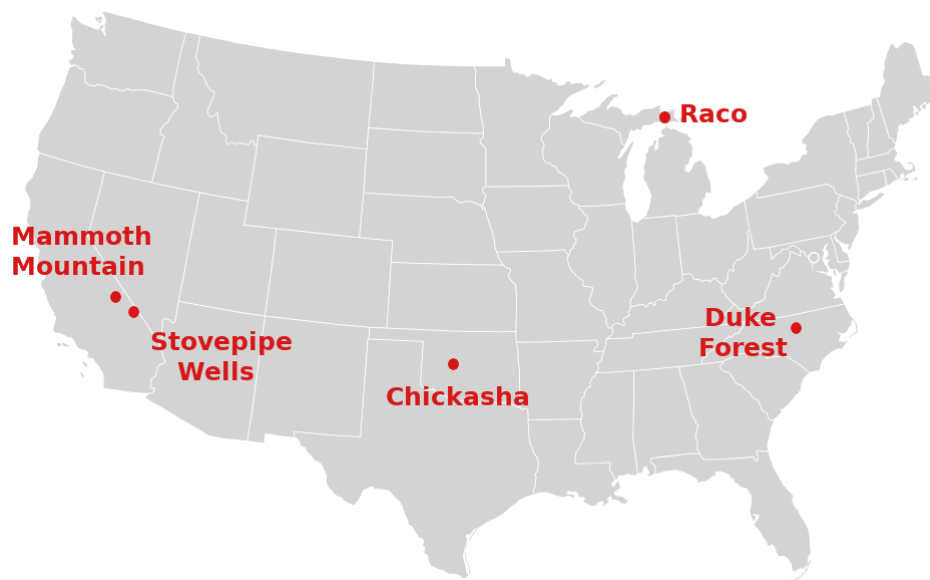


Figure 1: Map of locations of the SIR-C/X-SAR data used to create the database.

3 Data Preprocessing

The selected SIR-C/X-SAR data were calibrated into *single-look radar backscattering cross-section per unit area*, $\sigma^{(1)}$, using the calibration coefficients provided by the Jet Propulsion Laboratory (JPL) and DLR for the SIR-C and X-SAR data, respectively. These coefficients account for the antenna pattern, range-dependent spreading losses and SAR processor gains. In addition to these factors, the SAR data were preprocessed to account for the effects of terrain. Terrain (vertical relief) can cause serious distortions in SAR data due to the oblique viewing geometry; and simple conversion from slant- to ground-range projection can introduce both geometric and radiometric errors into the resultant image. Such geometric errors would make it difficult to accurately coregister the SAR data with ancillary land-cover information and could potentially lead to serious spatial errors in the construction of the database. The radiometric errors introduced via the common assumptions of either flat or curved-earth would also degrade the database. Fortunately, these errors are largely correctable by using a *digital elevation model* (DEM) to orthorectify the data. The terrain model was used to generate a new SAR image in a ground-range projection wherein the SAR data is repositioned in both range and azimuth to account for local relief, and the backscattering coefficient is area-corrected using local slope.

Two map datasets are needed to perform the orthorectification process: digital elevation and vector data of the network of roads /rivers. The elevation data are obtained from the U.S. Geological Survey (USGS) as either 1:100,000 digitized hypsography vectors or as 1:250,000 raster maps. The maps of roads, rivers, and hypsography vectors are the same as those found on 1:250,000 scale paper maps produced by the USGS. These vectors were manually digitized by the USGS and are provided in a vector format known as *Digital Line Graphs* (DLG). As for the land cover classification data, they come in small pieces ($1^\circ \times 1^\circ$) which were then mosaiced together over a larger area and then transformed to the appropriate *Universal Transverse Mercator* (UTM) map projection (using the NAD-27 horizontal datum). The elevation data were also transformed to a new vertical datum by changing them from mean sea level to the NAD-27 ellipsoid. The lower-resolution raster

Table 2: Examples of some of the source data selected for use in the database.

GENERAL CONDITIONS	REGION	SITE NAME	SIR-C/X-SAR DATA				
			Mission	Data-Take	CD-ROM	Angle	L+C-Quad?
Temperate Forest	North Carolina $\pm 2^\circ$ of 36° N, 79° W	Duke Forest 7 data-takes max. angular range = 18° to 44°	SRL-1	49.31	1-11	39.7	Y
				113.30	1-06	17.8	Y
				129.20	1-21	26.7	Y
				145.20	1-03	32.1	Y
			SRL-2	17.21	2-25	53.6	hh, hv, Xvv
				33.21	2-44	44.3	Y
				49.31	2-26	38.3	Y
	113.30	2-35		22.6	Y		
	Michigan $\pm 2^\circ$ of 46° N, 85° W	Raco 22 data-takes max. angular range = 20° to 42°	SRL-1	6.10	1-39	32.0	Y
				22.20	1-12	20.4	Y
				66.20	1-05	21.9	Y
				82.20	1-54	31.3	Y
				86.40	1-33	26.7	Y
				98.12	1-15	37.2	Y
				102.41	1-15	31.8	Y
				114.10	1-07	41.7	Y
			SRL-2	134.30	1-49	41.9	Y
				150.20	1-19	44.2	hh, hv, Xvv
				6.20	2-01	31.8	Y
				22.20	2-18	21.4	Y
				66.12	2-07	22.0	Y
				82.20	2-41	31.5	Y
86.40				2-08	26.5	Y	
98.20	2-04	37.9	Y				
102.41	2-27	37.3	Y				
114.10	2-55	43.4	Y				
118.31	2-02	40.6	Y				
134.31	2-03	40.6	Y				
150.31	2-05	40.6	Y				
166.30	2-47	40.2	Y				

elevation data were used only when the hypsography was not available and went through the same geometric transformations. The vector hypsography data was resampled to a raster grid with a 5 m pixel spacing. This raster image is used by the orthorectification procedure. The vector to raster transformation and resampling used the vectors to fill in elevations for those pixels that were touched by the vectors, and then using interpolation to provide elevations for the remaining pixels.

Orthorectification is the process wherein a SAR image is resampled to overlay it onto a map. Orthorectification of the SAR imagery is required in order to correctly register the SAR data to the ancillary land-cover classification data. The resampling of the SAR imagery is not merely a “rubber sheet” stretching of the image but also relies on accurate determination of the sensor orbit and the use of an accurate ground elevation map in order to account for all the distortions inherent in the SAR imaging process.

Some distortions cannot be fixed. These are induced when local vertical relief is too great relative to the sensor viewing angle. The distortions lead to layover and shadow. During the orthorectification process the local slope in the range direction is used to identify regions of layover and shadow. Such pixels are marked where appropriate to create masks of the layover and shadow regions. These pixels are not used in the covariance matrix calculations to generate radar backscatter pdfs. During orthorectification two angles are calculated: the local incidence angle, and the local slope angle. The **local angle of incidence**

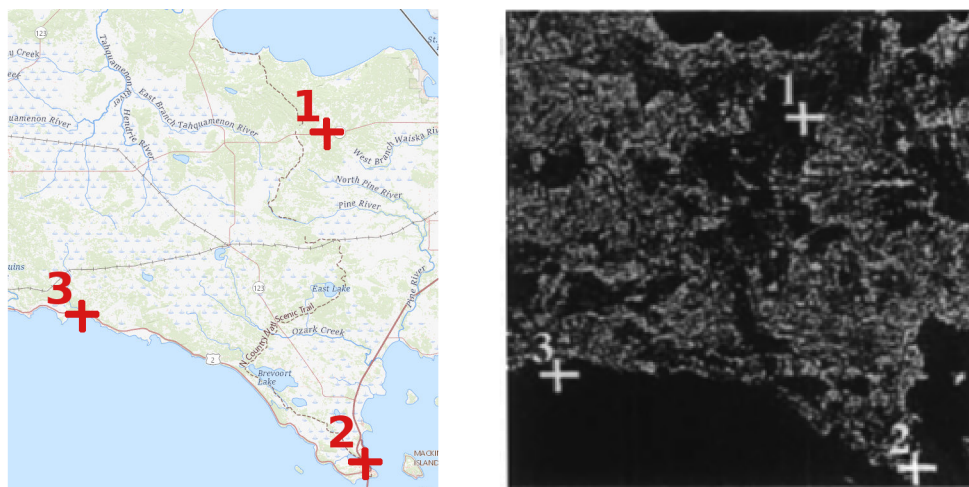


Figure 2: Ground control points are used to tie the SAR imagery to the DEM in the orthorectification process.

is defined as the angle between the normal to the ground and the incident radar wave. The local slope is the angle of the ground relative to horizontal in the plane of incidence. For details of the orthorectification geometry, see Curlander and McDonough [2]. To implement the orthorectification process, the SAR image must be accurately located with respect to the digital elevation model. The Digital Line Graph (DLG) vectors are used to find road intersections or other distinctive locations that are easy to locate in the SAR image. A manual process is used to identify a dozen or more ground control points, each with a known location on Earth and a known location in the SAR image. Given this set of ground control points, plus an initial guess of the sensor orbit (provided in the SAR data header), the orbit is optimized to produce the least error in the coregistration of the ground control points. Then, the orthorectification algorithm performs its corrections (radiometric and geometric) to the SAR image using the raster elevation map. The SAR image data are resampled to a raster grid that has the same coordinates and size as the elevation map, as shown in Figure 2. The process also produces two more images representing the presence of layover or shadow, the local incidence angle, and the ground slope angle.

Only a subset of 56 (of the available 152) SAR image scenes were selected for complete processing and use in the final backscatter database. A list of these SAR data sets is given in Table 3. This subset was selected to cover the range of available incidence angles for each site and the range of available scene conditions. Additionally, the scene selection was conditioned upon the provision of a statistically significant sample population of single-look pixels (more than 10,000) for each terrain class and local angle of incidence bin.

4 SIR-C SAR Database

Radar scattering by terrain is governed by two sets of parameters, the geophysical parameters of the scene—which include geometrical factors such as the shapes, sizes and orientations of the scattering elements contained in the illuminated scene, and the dielectric properties of those scattering elements—and three radar parameters: the radar frequency f , the antenna polarization configuration (hh, vv, or hv), and the local incidence angle θ (relative to the average surface plane of the scene). The SIR-C SAR consisted of fully polarimetric radars that operated at L-band ($f = 1.25$ GHz) and C-band (5.3 GHz) and a

Table 3: Inventory of SIR-C/X-SAR data fully processed and included in database.

Site Name	SRL-1/2	Data Take	Look Angle	Scene Numbers		Conditions
				SIR-C	X-SAR	
Raco, Michigan	1	61.1	31		12882,3	snow, frozen, unplanted
	1	22.2	20	12131,2	12131,2	snow, frozen, unplanted
	1	82.2	31	11284,5	11284,5	snow, frozen, unplanted
	1	114.1	42	12888,9	12888,9	snow, frozen, unplanted
	2	6.2	32	42322,3	42322,3	dry soil, liquid water, planted
	2	66.12	22	40989,90		dry soil, liquid water, planted
	2	82.2	31	41404,5	41404,5	dry soil, liquid water, planted
	2	114.1	43	41335,6	41335,6	dry soil, liquid water, planted
	2	134.31	41	41331,2	41331,2	wet soil, liquid water, planted
	Chickasha, Oklahoma	1	34	27	16810,1	16810,1
1		50.1	42	16814,5	16814,5	wet soil, liquid water, planted
1		66.1	50	16816,7	16816,7	wet soil, liquid water, planted
1		98.11	60	16824,5	16824,5	dry soil, liquid water, planted
1		103.31	42	16830,1	16830,1	dry soil, liquid water, planted
1		135.3	31	16836,7		dry soil, liquid water, planted
1		151.3	26	16840,1	16840,1	dry soil, liquid water, planted
2		34.11	28	48384,5	48384,5	dry soil, liquid water, unplanted
2		50.11	41	48390,1	48390,1	dry soil, liquid water, unplanted
Fresno, California		1	51.1	23	16884,5	16884,5
	1	51.1	23	16886,7		dry soil, liquid water, planted
	1	67.1	34	16898,9	16898,9	wet soil, liquid water, planted
	1	99	34	16908,9	16908,9	dry soil, liquid water, planted
	1	99	34	16910,1		dry soil, liquid water, planted
	2	67.1	34	44270,1	44270,1	wet soil, liquid water, planted
	2	83.11	34	44272,3	44272,3	wet soil, liquid water, planted
	Death Valley, CA	1	136.2	40	16928,9	16928,9
Oklahoma City, OK	1	50.1	42	17052,3		wet soil, liquid water, planted
Philadelphia, PA	1	49.31	31		17054,5	wet soil, liquid water, planted
New York City, NY	1	49.31	31	17054,5		wet soil, liquid water, planted
	1	49.31	31	17056,7		wet soil, liquid water, planted

single-polarization (vv) radar at X-band (9.6 GHz). For each of the imaged scenes used to create the radar database, the X-band SAR measured the power backscattered from each resolution cell contained in that scene. Then, by applying a calibration algorithm, the measured backscattered signal at X-band is converted into an estimate of the backscattering coefficient σ^0 (dB) by averaging the power backscattered from 60–100 adjacent single-look pixels. For the recorded polarimetric measurements at L- and C-bands, similar calibration and multipixel averaging processes are implemented but the output quantity is the *covariance matrix* \mathbf{C} , rather than the backscattering coefficient.

For a single-look pixel, the calibrated covariance matrix is given by

$$\mathbf{C} = \begin{bmatrix} S_{hh}S_{hh}^* & S_{hh}S_{vv}^* & S_{hh}S_{hv}^* \\ S_{vv}S_{hh}^* & S_{vv}S_{vv}^* & S_{vv}S_{hv}^* \\ S_{hv}S_{hh}^* & S_{hv}S_{vv}^* & S_{hv}S_{hv}^* \end{bmatrix} \quad (2)$$

where S_{hh} , S_{vv} , and S_{hv} are the *scattering amplitudes* measured by the radar system.

The subscript notation denotes the polarization configuration, with the *first subscript denoting the polarization of the receive antenna and the second subscript denoting the polarization of the transmit antenna*. Thus, S_{hv} is the scattering amplitude of a terrain target observed by a horizontally polarized receive antenna when illuminated by a vertically polarized transmit antenna.

In general, the covariance matrix contains $4 \times 4 = 16$ elements defined in terms of four scattering amplitudes: S_{hh} , S_{vv} , S_{hv} , and S_{vh} . However, for a radar operating in the backscatter configuration—which a SAR is, the reciprocity theorem demands that $S_{hv} = S_{vh}$ [3, p.168]. Consequently, the 3×3 matrix given by Eq. (2) is sufficient to capture all of the polarization scattering behavior of the target.

The three scattering amplitudes, S_{vv} , S_{hh} , and S_{hv} , are each a complex quantity composed of a magnitude and an associated phase angle. For S_{hh} , for example,

$$S_{hh} = |S_{hh}|e^{j\phi_{hh}}. \quad (3)$$

Using the form defined by Eq. (2), we now examine the various types of backscattering information that can be extracted from the covariance matrix \mathbf{C} .

4.1 Single-Look Backscattering Cross-Section per Unit Area $\sigma^{(1)}$

The three diagonal elements of \mathbf{C} are related to the single-look backscattering cross-section per unit area $\sigma_{hh}^{(1)}$, $\sigma_{vv}^{(1)}$, and $\sigma_{hv}^{(1)}$ as follows:

$$\sigma_{hh}^{(1)} = 4\pi|S_{hh}S_{hh}^*| = 4\pi|S_{hh}|^2, \quad (4a)$$

$$\sigma_{vv}^{(1)} = 4\pi|S_{vv}S_{vv}^*| = 4\pi|S_{vv}|^2, \quad (4b)$$

$$\sigma_{hv}^{(1)} = 4\pi|S_{hv}S_{hv}^*| = 4\pi|S_{hv}|^2. \quad (4c)$$

4.2 Single-Look Co-Pol Phase Difference $\phi_{hh-vv}^{(1)}$

In addition to extracting intensity information from matrix \mathbf{C} , we also can extract phase differences. The off-diagonal element $S_{hh}S_{vv}^*$ is equivalent to

$$\begin{aligned} S_{hh}S_{vv}^* &= |S_{hh}|e^{j\phi_{hh}^{(1)}}|S_{vv}|e^{-j\phi_{vv}^{(1)}} \\ &= |S_{hh}||S_{vv}|e^{j\phi_{hh-vv}^{(1)}}, \end{aligned} \quad (5)$$

with

$$\phi_{hh-vv}^{(1)} = \phi_{hh}^{(1)} - \phi_{vv}^{(1)}. \quad (6)$$

The quantity $\phi_{hh-vv}^{(1)}$ is the *single-look co-pol phase difference*.

Matrix \mathbf{C} is Hermetian because element (1,2) is the complex conjugate of element (2,1), and the same is true for elements (1,3) and (3,1), and also for (2,3) and (3,2). Hence, not all 9 elements of \mathbf{C} need to be stored in the radar database; the 9 elements can be reduced down to 6. Furthermore, experimental observations—supported by theoretical considerations—have shown that for randomly distributed targets like the terrain types under consideration in the present study, the cross-pol phase differences $\phi_{hh-hv}^{(1)}$ and $\phi_{vv-hv}^{(1)}$ are characterized by a uniform pdf over the full range $[0, 2\pi]$, which means that these two cross-pol phase differences contain no target-specific information [3, p. 213]. This is in contrast with the co-pol phase difference $\phi_{hh-vv}^{(1)}$ for which its pdf is not uniform and the parameters of its pdf (such as the mean value and standard deviation) do vary with terrain type and microwave frequency. Hence, we should retain either element (1,2) or (2,1) in \mathbf{C} so as to compute the co-pol phase difference, but we need not retain the cross-pol phase elements. In conclusion, we need to retain only the following five real-valued attributes of \mathbf{C} :

$$S_{hh}S_{hh}^*, S_{vv}S_{vv}^*, S_{hv}S_{hv}^*, |S_{hh}S_{vv}^*|, \text{ and } \phi_{hh-vv}^{(1)}.$$

For the X-band data, we only need to store $S_{vv}S_{vv}^*$ because only vv-polarization was acquired by the SIR-C X-SAR.

4.3 Backscattering Coefficient σ^0

Given a SAR image composed of N single-look pixels of a certain terrain class, we can readily compute two important attributes, namely estimates of the radar *backscattering coefficient* σ^0 and the associated *single-look standard deviation* $s^{(1)}$:

$$\sigma^0 = \langle \sigma^{(1)} \rangle \approx \frac{1}{N} \sum_{i=1}^N \sigma^{(1)}[i], \quad (7)$$

$$s^{(1)} = \left[\langle (\sigma^{(1)} - \sigma^0)^2 \rangle \right]^{1/2} = \left[\frac{1}{N} \sum_{i=1}^N (\sigma^{(1)}[i] - \sigma^0)^2 \right]^{1/2}, \quad (8)$$

where $\sigma^{(1)}[i]$ are the N single-look values defined by Eq. (4). Here, $s^{(1)}$ is the standard deviation of the population of N pixels. The standard deviation associated with the average of the N pixels (namely σ^0) is

$$s^{(N)} = \frac{s^{(1)}}{\sqrt{N}}. \quad (9)$$

For all values computed in this study, N exceeds 35, and in most cases its value is close to 100.

According to the values for $s^{(1)}$ and σ^0 extracted from the database for various combinations of terrain types, frequency bands, and polarization configurations, the ratio $s^{(1)}/\sigma^0$ varied between a low of around 1.0 to a high of around 2.2. For most targets with uniform physical properties, such as a water or soil surface, the ratio is close to 1. This means that the estimated values of the backscattering coefficients reported in this study are related to the computed mean value σ^0 by

$$\tilde{\sigma}^0 = \sigma^0 \pm s^{(N)} = \sigma^0 \pm \left(\frac{s^{(N)}}{\sigma^0} \right) \sigma^0 = \sigma^0 \left[1 \pm \frac{1}{\sqrt{N}} \left(\frac{s^{(1)}}{\sigma^0} \right) \right]. \quad (10)$$

For $s^{(1)}/\sigma^0 = 1$ and $N = 100$,

$$\tilde{\sigma}^0 = \sigma^0 [1 \pm 0.1]. \quad (11)$$

When expressed in dB, the computed backscattering coefficient is given by

$$\sigma^0[\text{dB}] = 10 \log \sigma^0, \quad (12)$$

and the counterpart of Eq. (11) is

$$\begin{aligned} \tilde{\sigma}^0[\text{dB}] &= 10 \log(0.9\sigma^0) \text{ to } 10 \log(1.1\sigma^0) \\ &\approx \sigma^0[\text{dB}] \pm 0.4 \text{ dB}. \end{aligned} \quad (13)$$

4.4 Co-Pol Phase Difference $\phi_{\text{hh-vv}}$

Upon averaging the single-look co-pol phase difference given by Eq. (6) among the N pixels, we obtain the *mean co-pol phase difference* $\phi_{\text{hh-vv}}$:

$$\phi_{\text{hh-vv}} = \frac{1}{N} \sum_{i=1}^N \phi_{\text{hh-vv}}^{(1)}[i]. \quad (14)$$

4.5 Terrain Texture

As noted later in Section 5.3, the radar backscatter from terrain exhibits two types of pixel-to-pixel variations, one associated with the sensor and another associated with the terrain. The sensor-related variation is *image speckle*, which is characteristic of all narrow-bandwidth coherent imaging sensors, including SAR systems. The terrain-related variation is *target texture*, which accounts for pixel-to-pixel changes in the physical properties of the terrain.

Because image speckle and target texture are statistically independent processes, the variance of the combination is the sum of the variances of the individual contributions. In terms of the standard deviation, the *combined single-look standard deviation* $s^{(1)}$ is related to the *radar image-speckle standard deviation* $s_r^{(1)}$ and to the *terrain texture standard deviation* $s_t^{(1)}$ by

$$s^{(1)} = \left[(s_r^{(1)})^2 + (s_t^{(1)})^2 \right]^{1/2}. \quad (15)$$

According to the theory of radar image speckle for terrain targets with statistical uniform properties, the single-look standard deviation $s_r^{(1)}$ is equal to the mean value, namely σ^0 [3, p. 182]:

$$s_r^{(1)} = \sigma^0. \quad (16)$$

Upon dividing both sides of Eq. (15) by σ^0 and then using Eq. (16), we obtain

$$\frac{s^{(1)}}{\sigma^0} = \left[1 + \left(\frac{s_t^{(1)}}{\sigma^0} \right)^2 \right]^{1/2}. \quad (17)$$

The two quantities $s^{(1)}$ and σ^0 are computed from the radar database using Eqs. (7) and (8), thereby allowing us to determine the *terrain texture standard deviation to mean ratio* $s_t^{(1)}/\sigma^0$:

$$\frac{s_t^{(1)}}{\sigma^0} = \left[\left(\frac{s^{(1)}}{\sigma^0} \right)^2 - 1 \right]^{1/2}. \quad (18)$$

5 Software Data Products

5.1 Data Identification Code

In the database, the radar parameters associated with a given site are defined by the *radar configuration* sequence:

$$R = (A1, A2, A3, N), \quad (19)$$

where

$$A1 = \begin{cases} 1 & \text{for L-band,} \\ 2 & \text{for C-band,} \\ 3 & \text{for X-band,} \end{cases}$$

$$A2 = \begin{cases} 1 & \text{for HH Polarization } \sigma^0 \text{ (dB) (for L- and C-bands only),} \\ 2 & \text{for VV Polarization } \sigma^0 \text{ (dB),} \\ 3 & \text{for HV Polarization } \sigma^0 \text{ (dB) (for L- and C-bands only),} \\ 4 & \text{for HH-VV Phase } \phi_{hh-vv} \text{ (for L- and C-bands only),} \end{cases}$$

$A3$ = incidence angle θ in degrees, relative to normal incidence,

N = number of looks.

The radar database exceeds 5 Gigabytes of data, so to facilitate the extraction of data products of relevance to specific applications of interest, a specialized *Graphical User Interface* (GUI) was developed and tested.

5.2 Terrain Identification Code

The Terrain Identification Code (TIC) is an exact match to the list provided in Table 1, except that the code consists of seven integers instead of just six. In the list below, the last digit is a zero (0) for all classes, so it is superfluous. It was included in the code when the classification system was established in 1999 just in case it proves needed in the future for further subdivision of the terrain classes.

L1	L2	L3	L4	L5	L6	L7	
1	0	0	0	0	0	0	Non-vegetated
1	1	0	0	0	0	0	Urban
1	1	1	0	0	0	0	Small Town
1	1	2	0	0	0	0	Large City
1	2	0	0	0	0	0	Water Bodies
1	2	1	0	0	0	0	Liquid Water
1	2	1	1	0	0	0	Calm
1	2	1	2	0	0	0	Moderate winds/waves
1	2	1	3	0	0	0	High winds/waves
1	2	2	0	0	0	0	Frozen (ice)
1	2	2	1	0	0	0	Smooth
1	2	2	2	0	0	0	Rough
1	3	0	0	0	0	0	Roads or paved surfaces (asphalt or concrete)
1	4	0	0	0	0	0	Bare Soil
1	4	0	0	1	0	0	Wet Soil
1	4	0	0	1	1	0	April
1	4	0	0	1	2	0	October
1	4	0	0	2	0	0	Dry Soil
1	4	0	0	2	1	0	April
1	4	0	0	2	2	0	October
2	0	0	0	0	0	0	Sparse Vegetation
2	1	0	0	2	0	0	Desert (dry soil)
2	1	1	1	2	0	0	Grasses (dry soil)
2	1	2	1	2	0	0	Shrubs (dry soil)
3	0	0	0	0	0	0	Dense Vegetation
3	1	0	0	1	0	0	Wetlands
3	1	1	1	1	0	0	Grasses (flooded)
3	1	2	2	1	0	0	Trees (flooded)
3	2	0	0	0	0	0	Grasses and Sedges
3	2	0	1	0	0	0	Short Grasses ($h < 25$ cm)
3	2	0	1	1	0	0	Wet soil
3	2	0	1	2	0	0	Dry soil
3	2	0	2	0	0	0	Tall Grasses ($h \geq 25$ cm)
3	2	0	2	1	0	0	Wet soil
3	2	0	2	2	0	0	Dry soil
3	3	0	0	0	0	0	Shrubs
3	3	0	1	0	0	0	Short Shrubs ($h < 1$ m)
3	3	0	1	1	0	0	Wet soil
3	3	0	1	2	0	0	Dry soil
3	3	0	2	0	0	0	Tall Shrubs ($h \geq 1$ m)
3	3	0	2	1	0	0	Wet soil
3	3	0	2	2	0	0	Dry soil

L1	L2	L3	L4	L5	L6	L7	
3	4	0	0	0	0	0	Trees
3	4	1	0	0	0	0	Needle-leaf
3	4	1	1	0	0	0	Short ($h < 5$ m)
3	4	1	1	1	0	0	Wet Soil
3	4	1	1	1	1	0	April
3	4	1	1	1	2	0	October
3	4	1	1	2	0	0	Dry Soil
3	4	1	1	2	1	0	April
3	4	1	1	2	2	0	October
3	4	1	1	3	0	0	Snow-covered soil
3	4	1	2	0	0	0	Tall ($h \geq 5$ m)
3	4	1	2	1	0	0	Wet Soil
3	4	1	2	1	1	0	April
3	4	1	2	1	2	0	October
3	4	1	2	2	0	0	Dry Soil
3	4	1	2	2	1	0	April
3	4	1	2	2	2	0	October
3	4	1	2	3	0	0	Snow-covered soil
3	4	2	0	0	0	0	Broadleaf
3	4	2	1	0	0	0	Short ($h < 5$ m)
3	4	2	1	1	0	0	Wet Soil
3	4	2	1	1	1	0	April
3	4	2	1	1	2	0	October
3	4	2	1	2	0	0	Dry Soil
3	4	2	1	2	1	0	April
3	4	2	1	2	2	0	October
3	4	2	1	3	0	0	Snow-covered soil
3	4	2	2	0	0	0	Tall ($h \geq 5$ m)
3	4	2	2	1	0	0	Wet Soil
3	4	2	2	1	1	0	April
3	4	2	2	1	2	0	October
3	4	2	2	2	0	0	Dry Soil
3	4	2	2	2	1	0	April
3	4	2	2	2	2	0	October
3	4	2	2	3	0	0	Snow-covered soil
3	4	3	0	0	0	0	Mixed needle/broadleaf
3	4	3	1	0	0	0	Short ($h < 5$ m)
3	4	3	1	1	0	0	Wet Soil
3	4	3	1	1	1	0	April
3	4	3	1	1	2	0	October
3	4	3	1	2	0	0	Dry Soil
3	4	3	1	2	1	0	April
3	4	3	1	2	2	0	October
3	4	3	1	3	0	0	Snow-covered soil
3	4	3	2	0	0	0	Tall ($h \geq 5$ m)
3	4	3	2	1	0	0	Wet Soil
3	4	3	2	1	1	0	April
3	4	3	2	1	2	0	October
3	4	3	2	2	0	0	Dry Soil
3	4	3	2	2	1	0	April
3	4	3	2	2	2	0	October
3	4	3	2	3	0	0	Snow-covered soil
3	4	4	0	0	0	0	Tropical Jungle
3	4	4	0	1	0	0	Lowland (wet soil)
3	4	4	0	2	0	0	Upland (dry soil)

5.3 Histograms for a Specific Terrain Category

Step 1: Use TIC of Section 5.2 to specify terrain category

TIC: -----

Step 2: Select angle of incidence range

- 20°–25°
- 25°–30°
- 30°–35°
- 35°–40°
- 40°–45°
- 45°–50°
- 50°–55°
- 55°–60°

Step 3: Select histogram format

- A** Tabular (see example in Table 4)
- B** Graphical

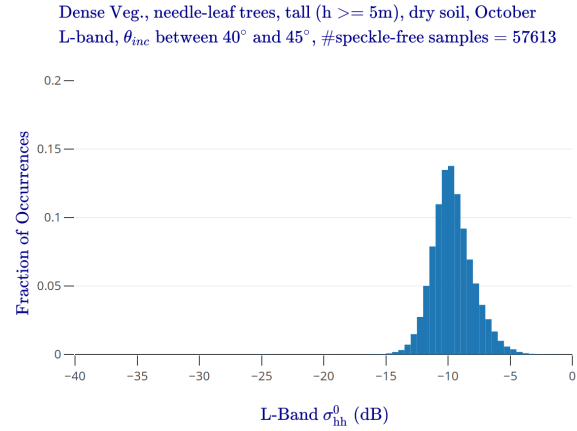
Step 3B: For graphical histogram, select all desired quantities.

- L-Band σ_{vv}^0 (dB)
- L-Band σ_{hh}^0 (dB)
- L-Band σ_{hv}^0 (dB)
- L-Band $\sigma_{hv}^0/\sigma_{vv}^0$ (dB)
- L-Band $\sigma_{hv}^0/\sigma_{hh}^0$ (dB)
- L-Band ϕ_{hh-vv} (degrees)
- C-Band σ_{vv}^0 (dB)
- C-Band σ_{hh}^0 (dB)
- C-Band σ_{hv}^0 (dB)
- C-Band $\sigma_{hv}^0/\sigma_{vv}^0$ (dB)
- C-Band $\sigma_{hv}^0/\sigma_{hh}^0$ (dB)
- C-Band ϕ_{hh-vv} (degrees)
- X-Band σ_{vv}^0 (dB)

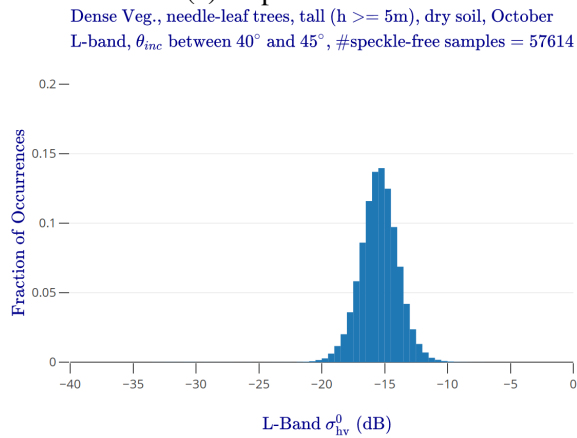
Examples of GUI-generated histograms are shown in Figures 3 and 4.

Table 4: Radar scattering histogram elements for dense vegetation category, needle-leaf trees with height > 5 m and dry soil, observed in October 1994 at incidence angles in the range 40° to 45° . All σ^0 values are in dB, and phase-difference values are in degrees.

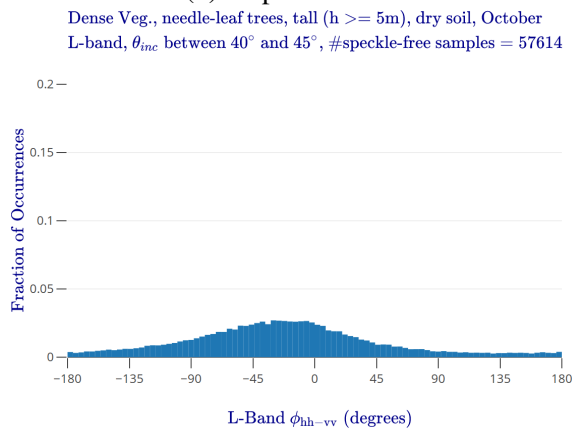
	σ_{\max}^0	σ_3^0	$\sigma_{2.5}^0$	Median	$\sigma_{7.5}^0$	σ_{95}^0	σ_{\min}^0	Mean	Std. Dev.	Sample Size
L-Band σ_{hh}^0 (dB)	-0.020246	-12.099401	-10.695248	-9.747843	-8.655583	-6.716163	-28.170151	-9.633027	1.678394	57613
L-Band σ_{vv}^0 (dB)	-2.345267	-13.801453	-12.357566	-11.419262	-10.451884	-8.826060	-25.920994	-11.382868	1.547748	57613
L-Band σ_{hv}^0 (dB)	-7.447396	-17.897083	-16.380079	-15.420424	-14.462504	-12.993915	-33.957741	-15.437838	1.563994	57614
L-Band ϕ_{hh-vv} (degrees)	179.983459	-136.446899	-66.487152	-24.190342	17.380180	116.998543	-179.991013	-21.049105	70.994390	57614
C-Band σ_{hh}^0 (dB)	-0.051424	-13.236723	-11.824743	-10.965573	-10.136180	-8.746619	-27.542406	-10.993454	1.481266	57613
C-Band σ_{vv}^0 (dB)	-2.026099	-13.344472	-11.917958	-11.040253	-10.187343	-8.775744	-25.720272	-11.061381	1.455820	57614
C-Band σ_{hv}^0 (dB)	-9.950127	-19.037506	-17.195581	-16.172087	-15.253758	-14.026778	-33.325470	-16.322165	1.642643	57614
C-Band ϕ_{hh-vv} (degrees)	179.918610	-56.632355	-19.576807	-0.226814	19.556583	57.572029	-179.978973	0.050503	37.303521	57614



(a) hh polarization

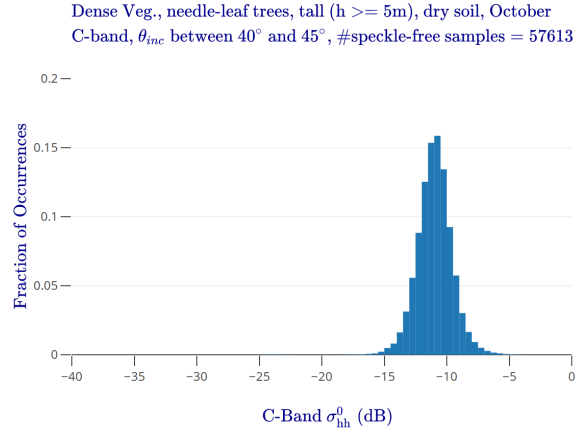


(b) hv polarization

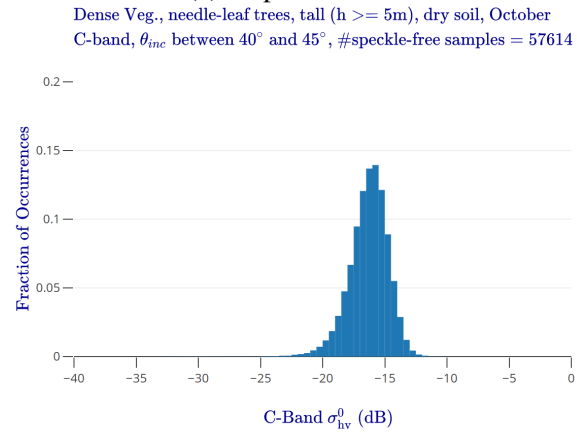


(c) Co-pol phase difference

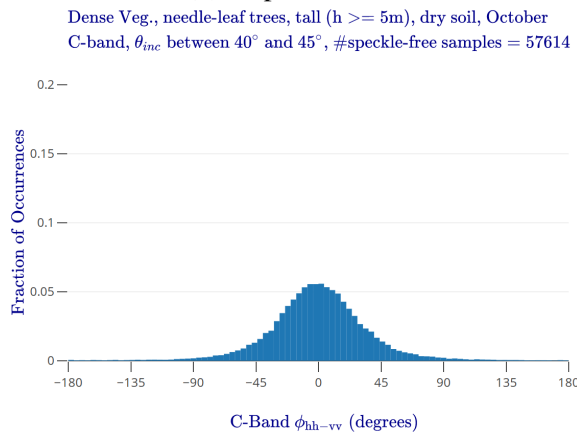
Figure 3: Histograms for dense vegetation category, needle-leaf trees with height $> 5\text{ m}$ and dry soil, observed in October 1994 at L-band and incidence angles in the range 40° to 45° .



(a) hh polarization



(b) hv polarization



(c) Co-pol phase difference

Figure 4: Histograms for dense vegetation category, needle-leaf trees with height $> 5\text{ m}$ and dry soil, observed in October 1994 at C-band and incidence angles in the range 40° to 45° .

5.4 Frequency Response at vv Polarization

The terrain swaths imaged by the L- and C-Band SARs were identical and essentially simultaneous. The X-Band imaging also occurred simultaneously, but its swath often overlapped with that of the L/C-Band SARs, but it was not identical. For terrain targets that were covered by all three frequency channels, we can generate frequency response plots by following the steps below:

Step 1: Use TIC of Section 5.2 to specify terrain category

TIC: - - - - -

Step 2: Select angle of incidence range

- 20°–25°
- 25°–30°
- 30°–35°
- 35°–40°
- 40°–45°
- 45°–50°
- 50°–55°
- 55°–60°

An example of a frequency plot is shown in Figure 5.

5.5 Scatter Plot

Upon selecting a terrain category and an angular range, the GUI can generate a scatter plot of any pair of radar parameters.

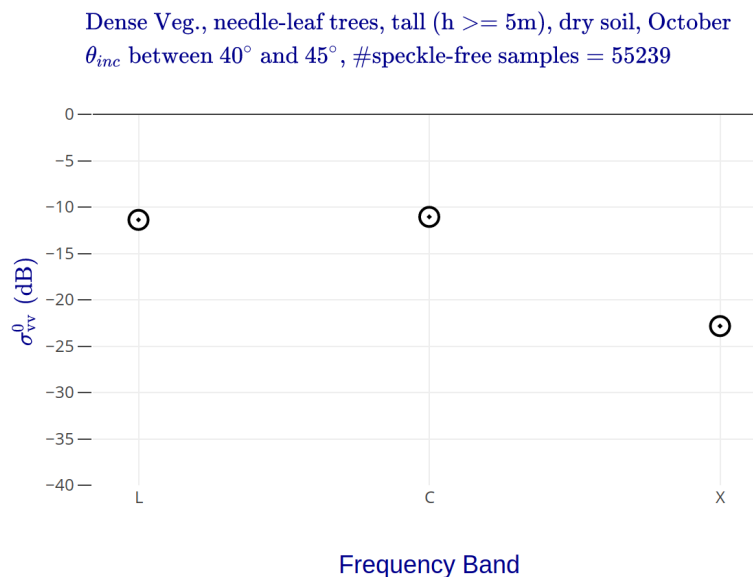


Figure 5: Frequency response for vv polarization for dense vegetation category, needle-leaf trees with height > 5 m and dry soil, observed in October 1994 at incidence angles in the range 40° to 45°.

Step 1: Use TIC of Section 5.2 to specify terrain category
TIC: -----

Step 2: Select angle of incidence range

- 20°–25°
- 25°–30°
- 30°–35°
- 35°–40°
- 40°–45°
- 45°–50°
- 50°–55°
- 55°–60°

Step 3: Select a pair of radar parameters

- L-Band σ_{vv}^0 (dB)
- L-Band σ_{hh}^0 (dB)
- L-Band σ_{hv}^0 (dB)
- L-Band $\sigma_{hv}^0/\sigma_{vv}^0$ (dB)
- L-Band $\sigma_{hv}^0/\sigma_{hh}^0$ (dB)
- L-Band ϕ_{hh-vv} (degrees)
- C-Band σ_{vv}^0 (dB)
- C-Band σ_{hh}^0 (dB)
- C-Band σ_{hv}^0 (dB)
- C-Band $\sigma_{hv}^0/\sigma_{vv}^0$ (dB)
- C-Band $\sigma_{hv}^0/\sigma_{hh}^0$ (dB)
- C-Band ϕ_{hh-vv} (degrees)

Figure 6 is an example of a scatter plot.

5.6 Radar Image Texture

Consider the single-look radar image shown in Figure 7. Each pixel represents a $5\text{ m} \times 5\text{ m}$ area in a field covered with short grass with wet soil. According to the TIC used in conjunction with Table 1, the terrain class is $T = [3, 2, 0, 1, 1, 0, 0]$. The image intensity represents the radar backscatter at L-band hh polarization. Even though all pixels in the image represent the same terrain class, we observe a fair amount of pixel-to-pixel variation. As noted in Section 4.5, the variation is due to two sources: (1) **radar speckle**, which is characteristic of any fully coherent electromagnetic sensor viewing a distributed target composed of a large number of randomly located scatterers—which is true for almost any natural surface or volume viewed by a SAR system, and (2) **target texture**, representing the natural spatial variation of the field’s physical properties (such as grass density, soil moisture variation, etc.). The target texture is represented by the terrain texture standard deviation to mean ratio ($s_t^{(1)}/\sigma^0$) given by Eq. (18). In Table 5, this quantity is calculated from the database for any specified terrain sequence T and radar configuration R (with $N = 1$).

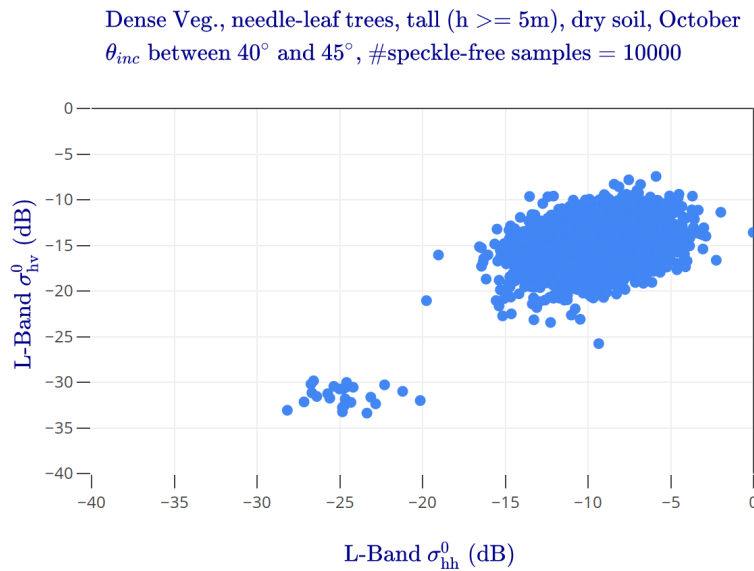


Figure 6: Scatter plot for hv backscattering coefficient versus hh backscattering coefficient for dense vegetation category, needle-leaf trees with height > 5 m and dry soil, observed in October 1994 at incidence angles in the range 40° to 45° .

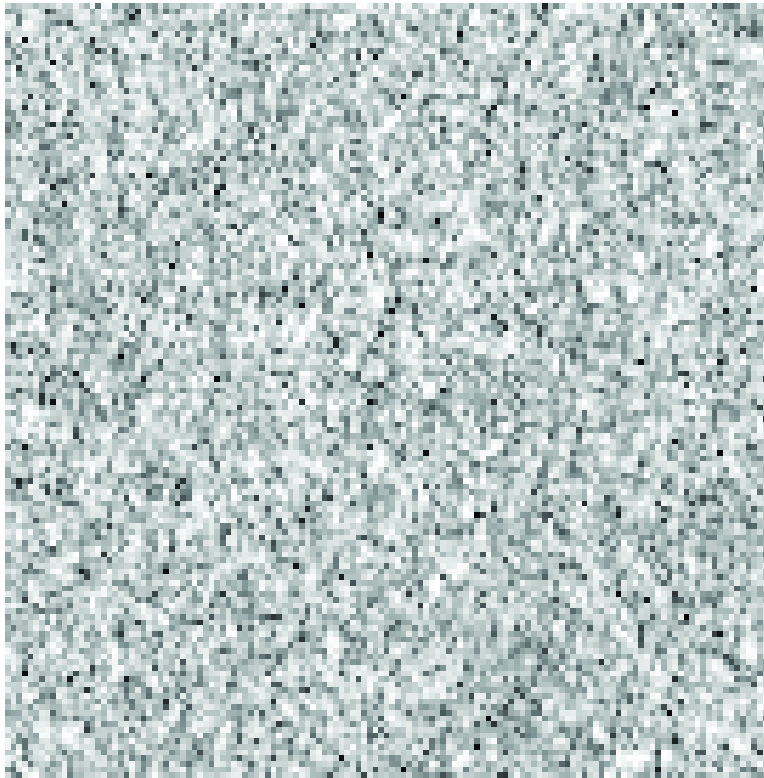


Figure 7: Single-look image with $5\text{ m} \times 5\text{ m}$ pixels. The pixel-to-pixel variation is due to a combination of radar speckle and spatial variations of the imaged scene. The imaged scene is tall needle-leaf trees over wet soil observed during the April mission at L-band and hh polarization.

References

- [1] Freeman, A., M. Zink, E. Caro, A. Moreira, L. Villeux, M. Werner, “The Legacy of the SIR-C/X-SAR Radar System: 25 Years On,” *Remote Sensing of Environment*, vol. 231, 2019.
- [2] Curlander, J. C. and R. N. McDonough, *Synthetic Aperture Radar and Signal Processing*, John Wiley & Sons, Inc., New York, 1991.
- [3] Ulaby, F. T. and D. G. Long, *Microwave Radar and Radiometric Remote Sensing*, Artech House, 2014.

Table 5: Single-look standard deviations to mean ratio: combined ($\sigma^{(1)}/\sigma^0$), radar ($\sigma_r^{(1)}/\sigma^0$), and terrain texture ($\sigma_t^{(1)}/\sigma^0$), all based on $5\text{ m} \times 5\text{ m}$ single-look pixels. Because theory mandates that the radar component $\sigma_r^{(1)}/\sigma^0 = 1$, if the combined $\sigma^{(1)}/\sigma^0$ is less than 1, it is rounded up to 1. The combined standard deviation is computed from the radar data, and the terrain texture standard deviation is computed using Eq. (18). Texture key: H = high, M = medium, L = low.

Terrain Type and Texture	Frequency Band	Polarization Configuration	Combined Standard Deviation to Mean Ratio $\sigma^{(1)}/\sigma^0$	Radar Standard Deviation to Mean Ratio $\sigma_r^{(1)}/\sigma^0$	Terrain Standard Deviation to Mean Ratio $\sigma_t^{(1)}/\sigma^0$
Urban H	L	HV	1.535	1	1.165
Urban M	L	HV	1.429	1	1.021
Urban L	L	HV	1.284	1	0.805
Suburban H	L	HV	1.667	1	1.334
Suburban M	L	HV	1.397	1	0.976
Suburban L	L	HV	1.340	1	0.892
Water1 H	L	HH	1.056	1	0.339
Water1 M	L	HH	1.029	1	0.243
Water1 L	L	HH	1	1	0
Water2 H	L	HH	1	1	0
Water2 M	L	HH	1.012	1	0.155
Water2 L	L	HH	1.009	1	0.134
Ice H	L	HH	1.845	1	1.550
Ice M	L	HH	2.226	1	1.989
Ice L	L	HH	1.035	1	0.267
Pavement	L	HV	1.026	1	0.230
Bare Soil Wet H	L	HV	1	1	0
Bare Soil Wet M	L	HV	1.125	1	0.515
Bare Soil Wet L	L	HV	1.408	1	0.991
Bare Soil Dry H	L	HV	2.095	1	1.841
Bare Soil Dry M	L	HV	1.582	1	1.226
Bare Soil Dry L	L	HV	1.460	1	1.064
Snow H	L	HH	1.210	1	0.681
Snow M	L	HH	1.389	1	0.964
Snow L	L	HH	1.034	1	0.263
Desert Shrubs H	L	HV	1	1	0
Desert Shrubs M	L	HV	1	1	0
Desert Shrubs L	L	HV	1.020	1	0.201
Swamp H	L	HV	1.681	1	1.351
Swamp M	L	HV	1.185	1	0.636
Swamp L	L	HV	1.018	1	0.191
Swamp Trees H	L	HV	1.157	1	0.582
Swamp Trees M	L	HV	1.038	1	0.278
Swamp Trees L	L	HV	1	1	0

Terrain Type and Texture	Frequency Band	Polarization Configuration	Combined Standard Deviation to Mean Ratio $\sigma^{(1)}/\sigma^0$	Radar Standard Deviation to Mean Ratio $\sigma_r^{(1)}/\sigma^0$	Terrain Standard Deviation to Mean Ratio $\sigma_t^{(1)}/\sigma^0$
Grass H	L	HV	1.170	1	0.607
Grass M	L	HV	1.087	1	0.426
Grass L	L	HV	1.066	1	0.369
Shrubs H	L	HV	1.478	1	1.088
Shrubs M	L	HV	1.402	1	0.983
Shrubs L	L	HV	1.203	1	0.669
Tall Needle-Leaf Trees Wet H	C	HV	1.061	1	0.355
Tall Needle-Leaf Trees Wet M	C	HV	1.044	1	0.300
Tall Needle-Leaf Trees Wet L	C	HV	1.037	1	0.275
Tall Needle-Leaf Trees Dry H	C	HV	1.160	1	0.588
Tall Needle-Leaf Trees Dry M	C	HV	1.118	1	0.500
Tall Needle-Leaf Trees Dry L	C	HV	1.045	1	0.303
Tall Needle-Leaf Trees Spring H	C	HV	1.085	1	0.421
Tall Needle-Leaf Trees Spring M	C	HV	1.063	1	0.361
Tall Needle-Leaf Trees Spring L	C	HV	1	1	0
Short Needle-Leaf Trees Wet H	C	HV	1.097	1	0.451
Short Needle-Leaf Trees Wet M	C	HV	1.048	1	0.314
Short Needle-Leaf Trees Wet L	C	HV	1.016	1	0.180
Short Needle-Leaf Trees Dry H	C	HV	1.246	1	0.743
Short Needle-Leaf Trees Dry M	C	HV	1.082	1	0.413
Short Needle-Leaf Trees Dry L	C	HV	1.033	1	0.259
Short Needle-Leaf Trees Spring H	C	HV	1.265	1	0.775
Short Needle-Leaf Trees Spring M	C	HV	1.061	1	0.355
Short Needle-Leaf Trees Spring L	C	HV	1	1	0
Tall Broad-Leaf Trees Wet H	C	HV	1.097	1	0.451
Tall Broad-Leaf Trees Wet M	C	HV	1.068	1	0.375
Tall Broad-Leaf Trees Wet L	C	HV	1.042	1	0.293

Terrain Type and Texture	Frequency Band	Polarization Configuration	Combined Standard Deviation to Mean Ratio $\sigma^{(1)}/\sigma^0$	Radar Standard Deviation to Mean Ratio $\sigma_r^{(1)}/\sigma^0$	Terrain Standard Deviation to Mean Ratio $\sigma_t^{(1)}/\sigma^0$
Tall Broad-Leaf Trees Dry H	C	HV	1.166	1	0.600
Tall Broad-Leaf Trees Dry M	C	HV	1.158	1	0.584
Tall Broad-Leaf Trees Dry L	C	HV	1.042	1	0.293
Tall Broad-Leaf Trees Spring H	C	HV	1.131	1	0.528
Tall Broad-Leaf Trees Spring M	C	HV	1.071	1	0.383
Tall Broad-Leaf Trees Spring L	C	HV	1.025	1	0.225
Mixed Trees Wet H	C	HV	1.087	1	0.426
Mixed Trees Wet M	C	HV	1.085	1	0.421
Mixed Trees Wet L	C	HV	1	1	0
Mixed Trees Dry H	C	HV	1.349	1	0.905
Mixed Trees Dry M	C	HV	1.048	1	0.314
Mixed Trees Dry L	C	HV	1	1	0
Mixed Trees Spring H	C	HV	1.532	1	1.161
Mixed Trees Spring M	C	HV	1.058	1	0.345
Mixed Trees Spring L	C	HV	1.065	1	0.366